Intrinsic stimuli-responsive main-chain supramolecular polymers driven by dative B←N bonds

Xupeng Ji,[a] Zihao Wang,[a] Wei Yuan,[b] Zhao Gao[a] and Wei Tian*[a]*

[a]*Shaanxi Key Laboratory of Macromolecular Science and Technology, Xi'an Key Laboratory of Hybrid Lumines-cent Materials and Photonic Device, MOE Key Laboratory of Material Physics and Chemistry under Extraordinary Conditions, School of Chemistry and Chemical Engineering, Northwestern Polytechnical University, Xi'an, 710072, China Xi'an, 710072, P. R. China*
[b]*Department of Chemistry, National University of Singapore 3 Science Drive 3, Singapore 117543, Singapore*
E-mail: gaozhao@nwpu.edu.cn; happytw_3000@nwpu.edu.cn.

Supporting Information

1. Materials and methods

Phenylboronic acid, 1,2-dihydroxybenzene, 1,4-phenylenediboronic acid, poly(dimethylsiloxane), bis(3-aminopropyl) terminated and dodecylamine were purchased form Energy Chemical, China. 1-(3-Dimethylaminopropyl)-3-ethylcarbodiimide hydrochloride (EDC·HCl) and 4-dimethylaminopyridine (DMAP)was purchased form J&K Scientific Ltd, China. 4-(Pyrid-4-yl)benzoic acid, 4-(1H-imidazol-1-yl)benzoic acid and TBAF (1M in THF) were purchased form Adamas, China. Boron trifluoride diethyl etherate (BTE, 46.5%), trifluoroacetic acid (TFA) and triethylamine (TEA) were purchased from Inno-Chem, China. All other reagents and solvents used in the experiments were obtained from commercial suppliers and used without further purification. All agents were used as received unless special statement.

^{1}H NMR, ^{13}C NMR and ^{11}B NMR spectra were obtained from Bruker Avance 400 instruments. Diffusion-ordered spectroscopy (DOSY) were obtained from Bruker Avance 600 instruments. High-resolution mass spectrometry was obtained using a LCMS-IT-TOF (Shimadzu, Japan) with suitable solvent, equipped with an ESI and APCI interface and an ion trap analyzer. The mass spectrometry of polymer was obtained using a MALDI-TOF-MS (Bruker Ultraflextreme). Fourier transform infrared (FT-IR) spectra were collected using a Spectrum Frontier FTIR spectrometer (Perkin Elmer, USA). Viscosity measurements were carried out with Ubbelohde semi-micro dilution viscometer (Shanghai Liangjing Glass Instrument Factory, 0.37 mm inner diameter) at 25°C in $CHCl_3$. Molecular weight distributions were measured on a conventional gel permeation chromatography (GPC) system equipped with a PL-GPC 50 (Agilent, USA).

Energy levels, frontier molecular orbital diagrams and energy distribution calculations. The optimized structures of $\mathbf{B_1}$, $\mathbf{N_{11}}$, $\mathbf{N_{12}}$, $\mathbf{B_1\text{-}N_{11}}$ and $\mathbf{B_1\text{-}N_{12}}$ were computed using the G09 software package.[1] The B3LYP/6-311G(d) basis set was employed to describe all elements. The energy levels of the highest occupied molecular orbital (HOMO) and lowest unoccupied molecular orbital (LUMO) were extracted from the optimized geometries. No imaginary frequencies were observed, confirming

that the optimized geometries correspond to true energy minima. To visually observe the dative B←N bonds between **B1** and **N11** (**N12**), the IGMH methods derived from DFT calculations were applied. The M06-2X functional[2] and the B3LYP/6-311G(d) basis set was adopted for all calculations. The DFT-D3 with BJ-damping[3] was applied to correct the weak interactions to improve the calculation accuracy. Then, the energy distribution mapping of optimized structures with color-mapped IGMH isosurfaces graphs of **B1-N11** and **B1-N12** were obtained. The binding energy (BE) between **B1** and **N11** (**N12**) was calculated based on the following Equation (Taking **B1-N11** for example):

$$\mathrm{BE} = E_{\mathbf{B_1-N_{11}}} - \left(E_{\mathbf{B_1}} + E_{\mathbf{N_{11}}}\right) \qquad \text{Eq. 1}$$

where $E_{\mathbf{B_1-N_{11}}}$ is the energy of entire molecule consisting of **B1-N11**, $\mathrm{E}_{\mathbf{B_1}}$ is the energy of **B1** and $E_{\mathbf{N_{11}}}$ is the energy of **N11**. Based on these methods, the value of the B←N bond energy was calculated.

The 1:1 binding model for **B1** and **N11** (**N12**) was determined by the titration experiments. To obtain the binding affinities, the shifts of the aromatic proton versus concentration in ^{1}H NMR spectra was solved by the following 1:1 binding equations[4]:

$$\Delta\delta = \delta_{\Delta BN}\left(\frac{[BN]}{[B]_0}\right) \qquad \text{Eq. 2}$$

$$[BN] = \frac{1}{2}\left\{\left([N]_0 + [B]_0 + \frac{1}{K_a}\right) - \sqrt{\left([N]_0 + [B]_0 + \frac{1}{K_a}\right)^2 - 4[B]_0[N]_0}\right\} \qquad \text{Eq. 3}$$

2. Synthetic routes to the monomers ***B₁, B₂, N₁₁, N₁₂, N₂₁, and N₂₂***

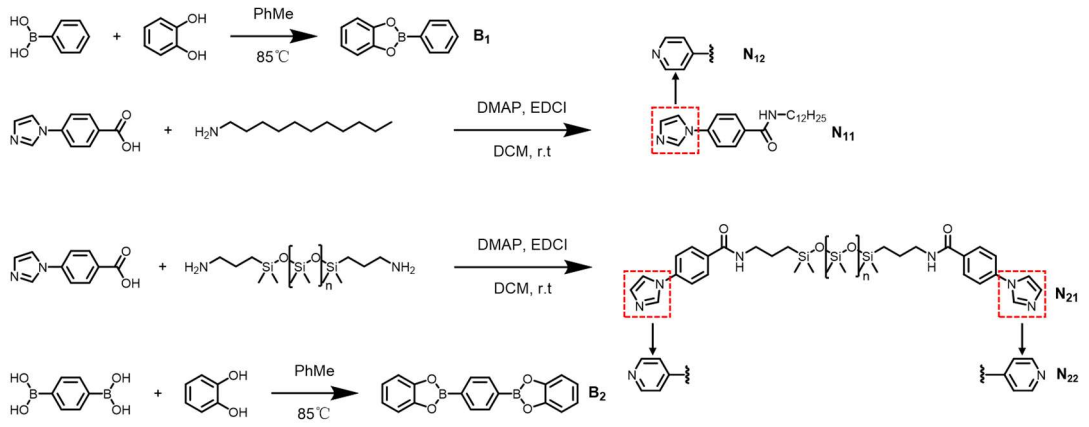

Scheme S1. Synthetic routes to the monomers $\mathbf{B_1}$, $\mathbf{B_2}$, $\mathbf{N_{11}}$, $\mathbf{N_{12}}$, $\mathbf{N_{21}}$, and $\mathbf{N_{22}}$.

2.1 Synthesis of the monomer $\boldsymbol{B_2}$

To a mixture of 1,4-phenylenediboronic acid (0.1011 g, 0.61 mmol) and 1,2-dihydroxybenzene (0.1402 g, 1.27 mmol) was added 40.00 mL of PhMe and 4.00 mL of MeOH. The solution was heated at reflux for 90 min and loaded half full with a 3 Å sieve in a Dean-Stark trap. Keep replenishing the methanol. During this time, a white solid begins to precipitate from the solution. The solution was evaporated to dryness, washed with petroleum ether and dried for 12 h. The pure product $\mathbf{B_2}$ as white solid (0.1712 g, 0.54 mmol, 89.7%) was obtained. ^{1}H NMR (400 MHz, $CDCl_3$) δ 8.14 (s, 2H), 7.28 (dd, J = 5.9, 3.4 Hz, 2H), 7.09 (dd, J = 5.8, 3.3 Hz, 2H). ^{11}B NMR (128 MHz, $CDCl_3$) δ 29.56.

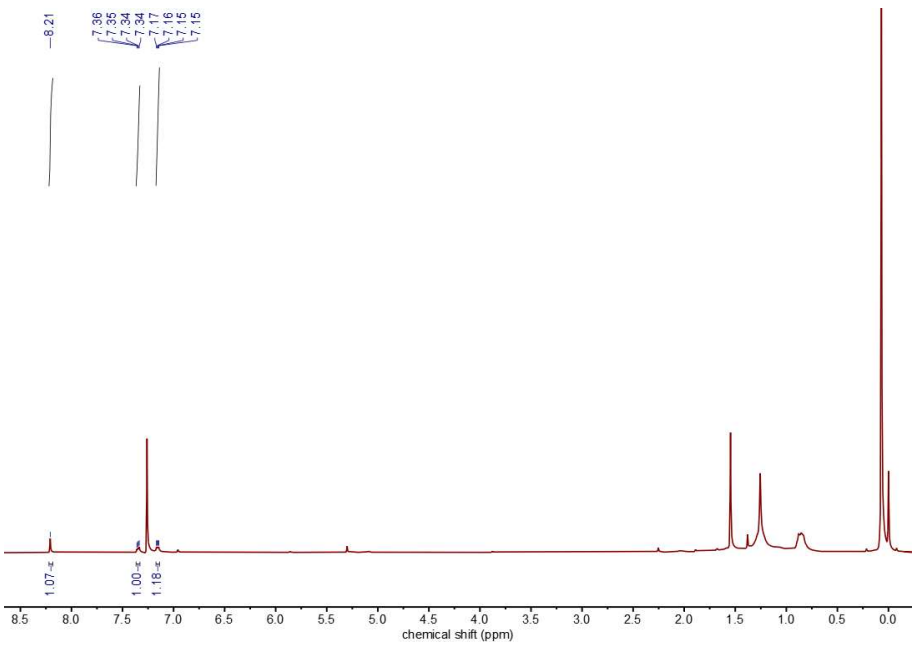

Figure S1. ^{1}H NMR spectrum (400 MHz, $CDCl_3$, 298 K, 2 mM) of the monomer $\mathbf{B_2}$.

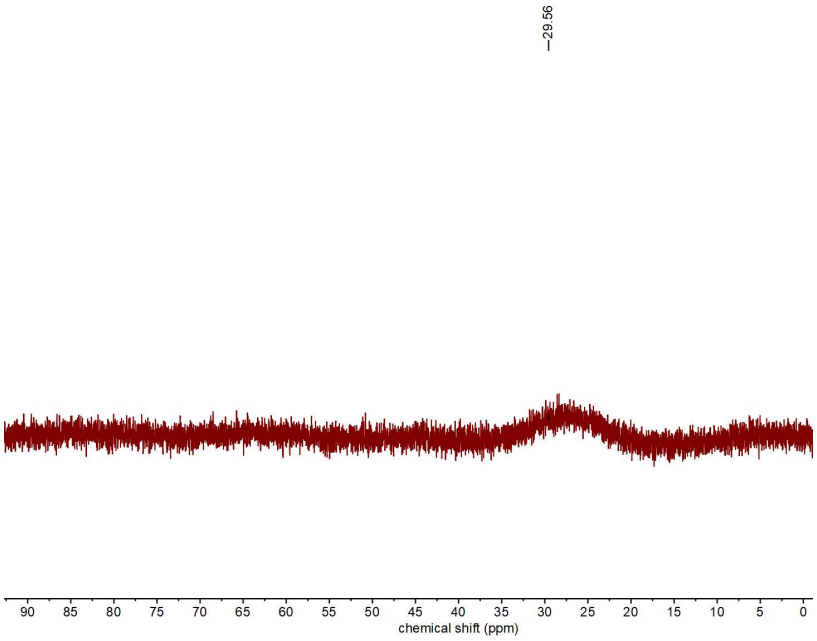

Figure S2. ^{11}B NMR spectrum (128 MHz, $CDCl_3$, 298 K, 2 mM) of the monomer $\mathbf{B_2}$.

2.2 Synthesis of the monomer $\boldsymbol{N_{21}}$

4-(1H-imidazol-1-yl)benzoic acid (0.3783 g, 2.01 mmol), DMAP (0.0820 g, 0.64 mmol), EDC·HCl (0.6729 g, 3.51 mmol) and DCM (40.00 mL) were stirred at room temperature for 30 min, and then dodecylamine (2.8500 g, 0.95 mmol) was added into the mixture. After stirring at room temperature for 12 h, the mixed solution was extracted two to three times with water/DCM and separated by column chromatography

(ethyl acetate/petroleum ether as eluent) to give **N21** as a pale yellow oily liquid (2.295 g, 0.675 mmol, 71.1%). ^{1}H NMR (400 MHz, $CDCl_3$) δ 7.93 (s, 2H), 7.90 (d, J = 8.1 Hz, 4H), 7.46 (d, J = 8.2 Hz, 4H), 7.33 (s, 2H), 7.24 (s, 2H), 6.24 (s, 2H), 3.47 (q, J = 6.9 Hz, 4H), 0.64–0.59 (m, 5H), 0.07 (s, 411H). ^{13}C NMR (101 MHz, $CDCl_3$) δ 165.00, 138.45, 134.40, 132.75, 129.87, 127.75, 119.94, 116.88, 42.00, 28.68, 22.57, 14.45, 0.07.

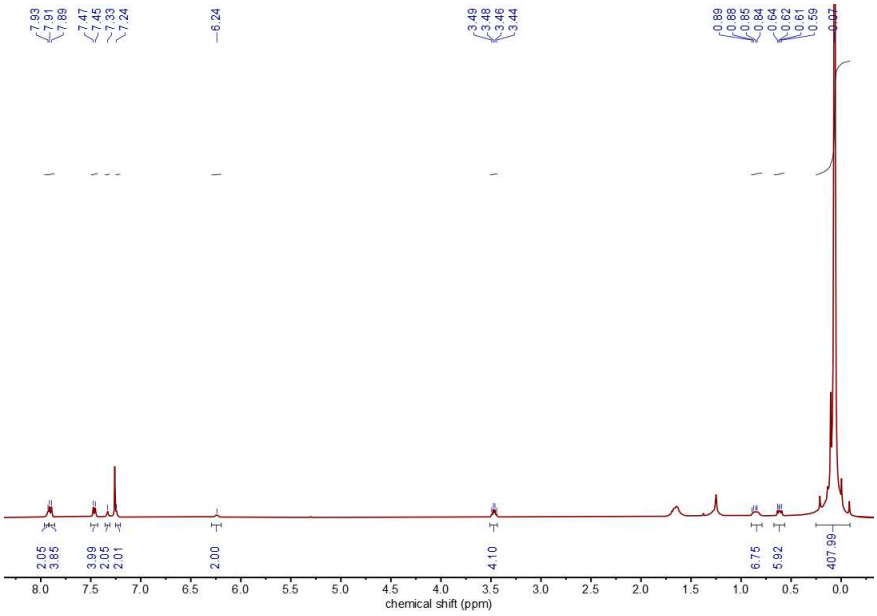

Figure S3. ^{1}H NMR spectrum (400 MHz, $CDCl_3$, 298 K, 2 mM) of the monomer **N21**.

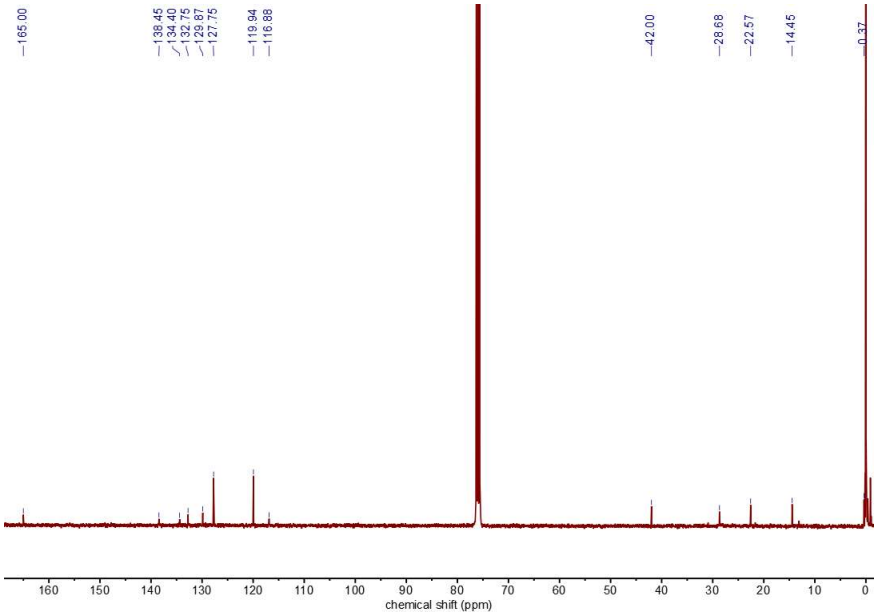

Figure S4. ^{13}C NMR spectrum (101 MHz, $CDCl_3$, 298 K, 15 mM) of the monomer **N21**.

2.3 Synthesis of the monomer ***N₂₂***

4-(Pyrid-4-yl)benzoic acid (0.4022 g, 2.02 mmol), DMAP (0.0807 g, 0.63 mmol), EDC·HCl (0.6845 g, 3.57 mmol) and DCM (40.00 mL) were stirred at room temperature for 30 min, and then dodecylamine (2.88 g, 0.96 mmol) was added into the mixture. After stirring at room temperature for 12 h, the mixed solution was extracted two to three times with water/DCM and separated by column chromatography (ethyl acetate/petroleum ether as eluent) to give **N_{22}** as a pale-yellow oily liquid (2.5110 g, 0.73 mmol, 76.5%). ^{1}H NMR (400 MHz, $CDCl_3$) δ 8.69 (d, J = 4.8 Hz, 4H), 7.89 (d, J = 8.3 Hz, 4H), 7.70 (d, J = 8.2 Hz, 4H), 7.52 (d, J = 5.8 Hz, 4H), 6.27 (s, 2H), 3.48 (q, J = 6.8 Hz, 4H), 1.73–1.65 (m, 4H), 0.65–0.58 (m, 4H), 0.07 (s, 356H). ^{13}C NMR (101 MHz, $CDCl_3$) δ 166.72, 150.44, 147.30, 141.03, 135.37, 127.74, 127.23, 121.82, 43.03, 23.68, 15.55, 1.06.

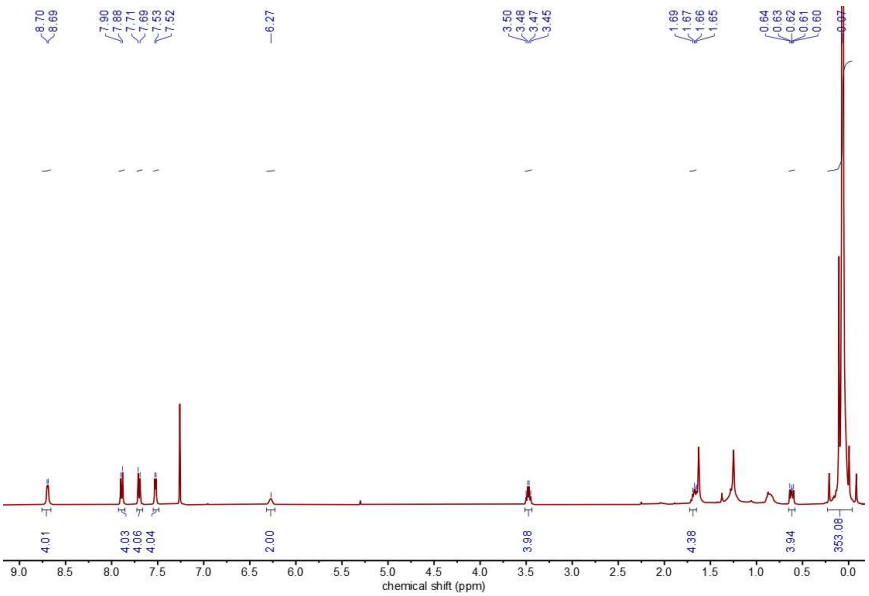

Figure S5. ^{1}H NMR spectrum (400 MHz, $CDCl_3$, 298 K, 2 mM) of the monomer **N_{22}**.

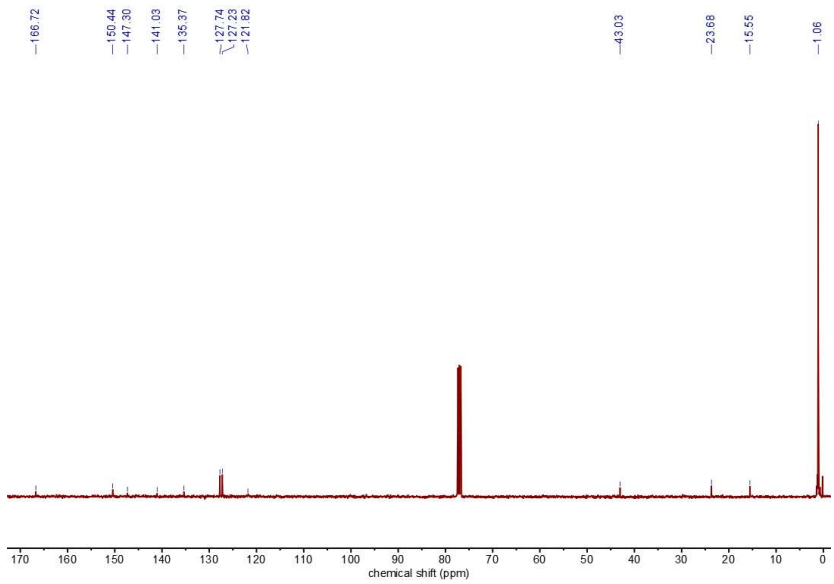

Figure S6. ^{13}C NMR spectrum (101 MHz, $CDCl_3$, 298 K, 15 mM) of the monomer $\mathbf{N_{22}}$.

2.4 Synthesis of the monomer $\boldsymbol{B_1}$

To a mixture of phenylboronic acid (0.1280 g, 1.04 mmol) and 1,2-dihydroxybenzene (0.1104 g, 1.00 mmol) was added 40.00 mL of PhMe and 4.00 mL of MeOH. The solution was heated at reflux for 90 min and loaded half full with a 3 Å sieve in a Dean-Stark trap. Keep replenishing the methanol. During this time, a white solid begins to precipitate from the solution. The solution was evaporated to dryness, washed with petroleum ether and dried for 12 h. The pure product $\mathbf{B_1}$ as white solid (0.1882 g, 0.96 mmol, 92.3%) was obtained. ^{1}H NMR (400 MHz, $CDCl_3$) δ 8.09 (d, J = 6.8 Hz, 2H), 7.58 (t, J = 7.4 Hz, 1H), 7.49 (t, J = 7.3 Hz, 2H), 7.32 (dd, J = 5.8, 3.4 Hz, 2H), 7.13 (dd, J = 5.8, 3.3 Hz, 2H). ^{11}B NMR (128 MHz, $CDCl_3$) δ 32.04.

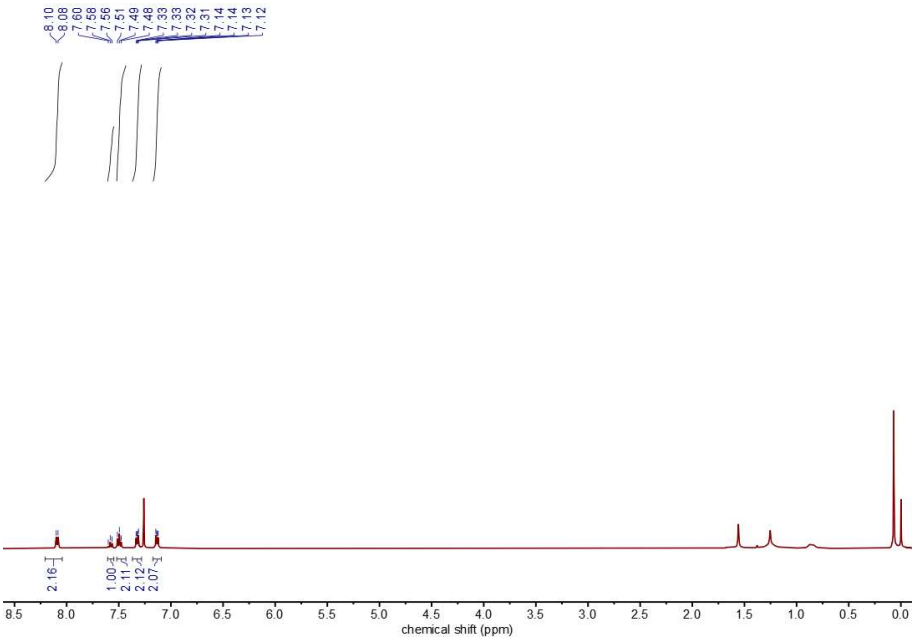

Figure S7. ^{1}H NMR spectrum (400 MHz, $CDCl_3$, 298 K, 2 mM) of the monomer $\mathbf{B_1}$.

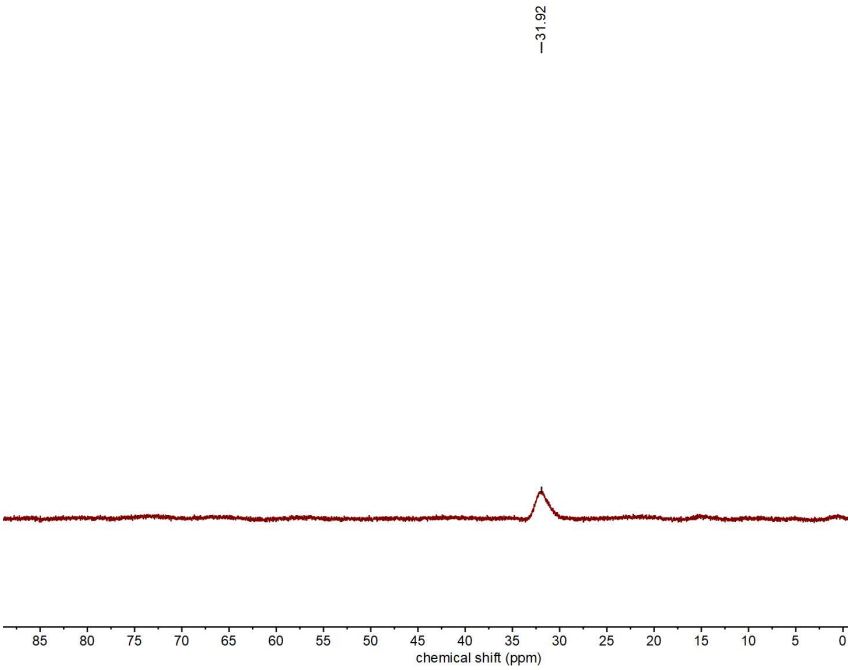

Figure S8. ^{11}B NMR spectrum (128 MHz, $CDCl_3$, 298 K, 2 mM) of the monomer $\mathbf{B_1}$.

2.5 Synthesis of the monomer $\boldsymbol{N_{11}}$

4-(1H-imidazol-1-yl)benzoic acid (0.1976 g, 1.05 mmol), DMAP (0.0410 g, 0.32 mmol), EDC·HCl (0.2895 g, 1.51 mmol) and DCM (40.00 mL) were stirred at room temperature for 30 min, and then dodecylamine (0.32 mL, 1.43 mmol) was added into the mixture. After stirring at room temperature for 12 h, the mixed solution was

extracted two to three times with water/DCM and separated by column chromatography (ethyl acetate/petroleum ether as eluent) to give **N11** as a white solid (0.2878 g, 0.81 mmol, 77.1%). ^{1}H NMR (400 MHz, $CDCl_3$) δ 7.94 (s, 1H), 7.89 (d, J = 8.5 Hz, 2H), 7.47 (d, J = 8.5 Hz, 2H), 7.34 (s, 1H), 7.25 (s, 1H), 6.15–6.09 (m, 1H), 3.47 (q, J = 6.9 Hz, 2H), 1.67–1.58 (m, 2H), 1.26 (s, 20H), 0.87 (t, J = 6.8 Hz, 3H). ^{13}C NMR (101 MHz, $CDCl_3$) δ 166.17, 139.56, 133.84, 131.01, 128.80, 128.65, 121.02, 117.91, 40.33, 31.95, 29.70, 29.68, 29.67, 29.63, 29.59, 29.53, 29.37, 27.06, 22.72, 14.15. ESI-MS (*m/z*): $[M + H]^+$, $C_{22}H_{33}N_3O$, calculated 356.2697; found 356.2960.

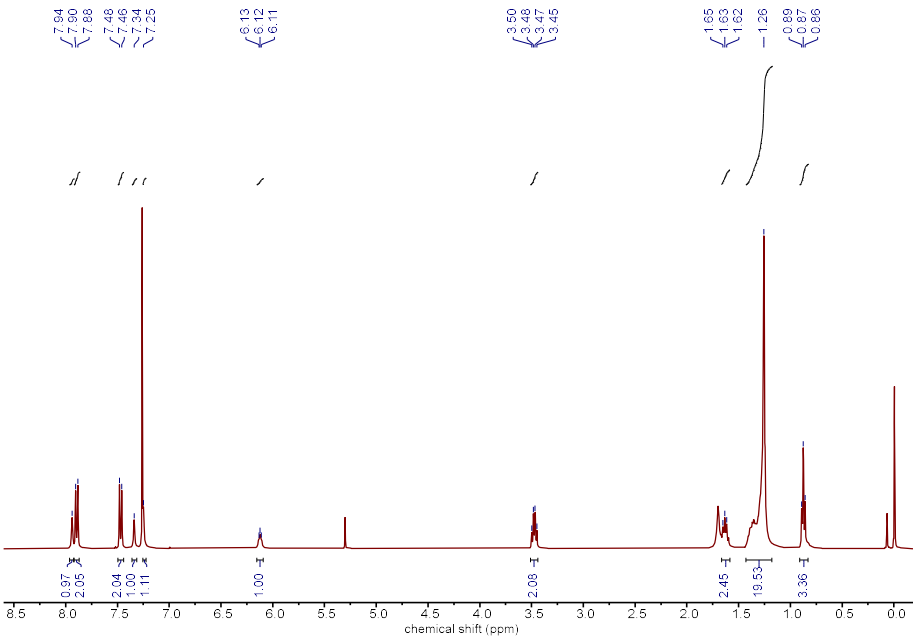

Figure S9. ^{1}H NMR spectrum (400 MHz, $CDCl_3$, 298 K, 2 mM) of the monomer $\mathbf{N_{11}}$.

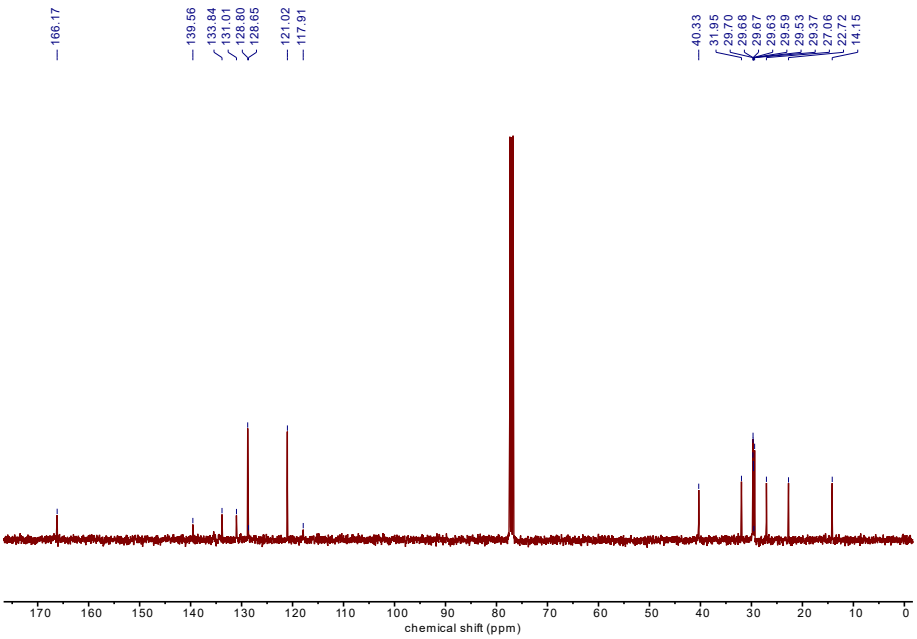

Figure S10. ^{13}C NMR spectrum (101 MHz, $CDCl_3$, 298 K, 15 mM) of the monomer $\mathbf{N_{I1}}$.

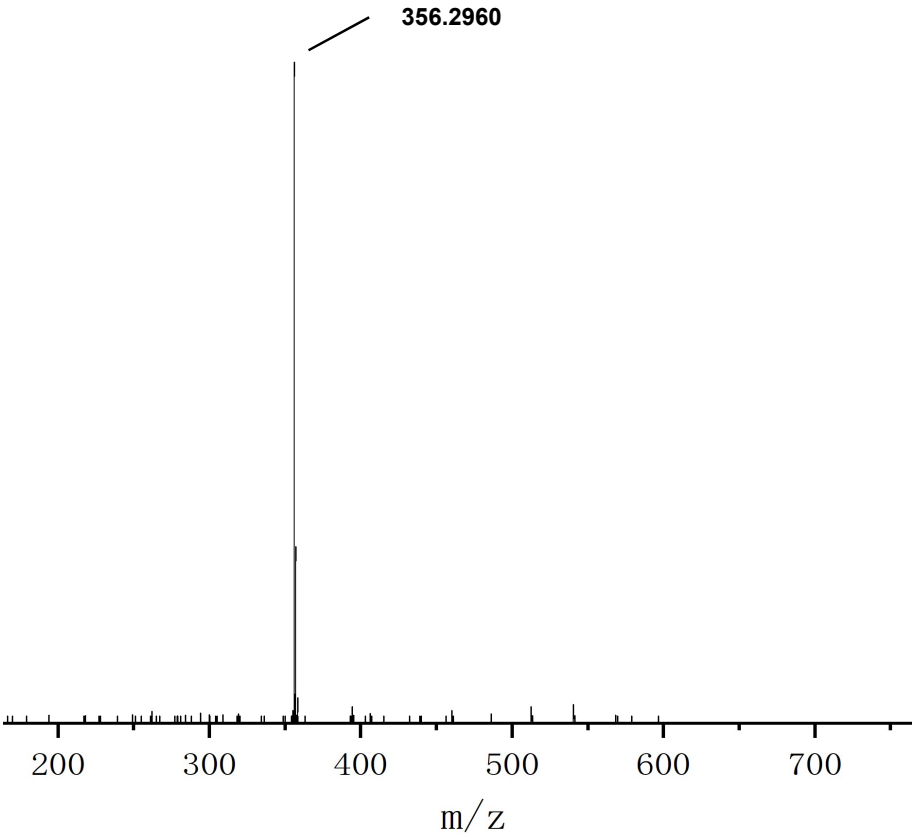

Figure S11. ESI-MS spectrum of the monomer $\mathbf{N_{I1}}$.

2.6 Synthesis of the monomer ***N12***

4-(Pyrid-4-yl)benzoic acid (0.2011 g, 1.01 mmol), DMAP (0.0397 g, 0.31 mmol), EDC·HCl (0.2857 g, 1.49 mmol) and DCM (40.00 mL) were stirred at room temperature for 30 min, and then dodecylamine (0.34 mL, 1.51 mmol) was added into the mixture. After stirring at room temperature for 12 h, the mixed solution was extracted two to three times with water/DCM and separated by column chromatography (ethyl acetate/petroleum ether as eluent) to give **N12** as a pale yellow solid (0.2894 g, 0.79 mmol, 78.2%). ^{1}H NMR (400 MHz, $CDCl_3$) δ 8.70 (d, J = 5.8 Hz, 2H), 7.88 (d, J = 8.2 Hz, 2H), 7.70 (d, J = 8.3 Hz, 2H), 7.54 (d, J = 6.0 Hz, 2H), 6.17 (s, 1H), 3.48 (q, J = 6.9 Hz, 2H), 1.64 (p, J = 7.4 Hz, 2H), 1.26 (s, 21H), 0.88 (t, J = 6.7 Hz, 4H). ^{13}C NMR (101 MHz, $CDCl_3$) δ 166.81, 150.45, 147.29, 141.02, 135.36, 127.73, 127.24, 121.68, 40.28, 31.95, 29.73, 29.68, 29.68, 29.67, 29.63, 29.59, 29.38, 27.06, 22.72, 14.15. ESI-MS (*m/z*): $[M + H]^+$, $C_{24}H_{34}N_2O$, calculated 367.2744; found 367.2743.

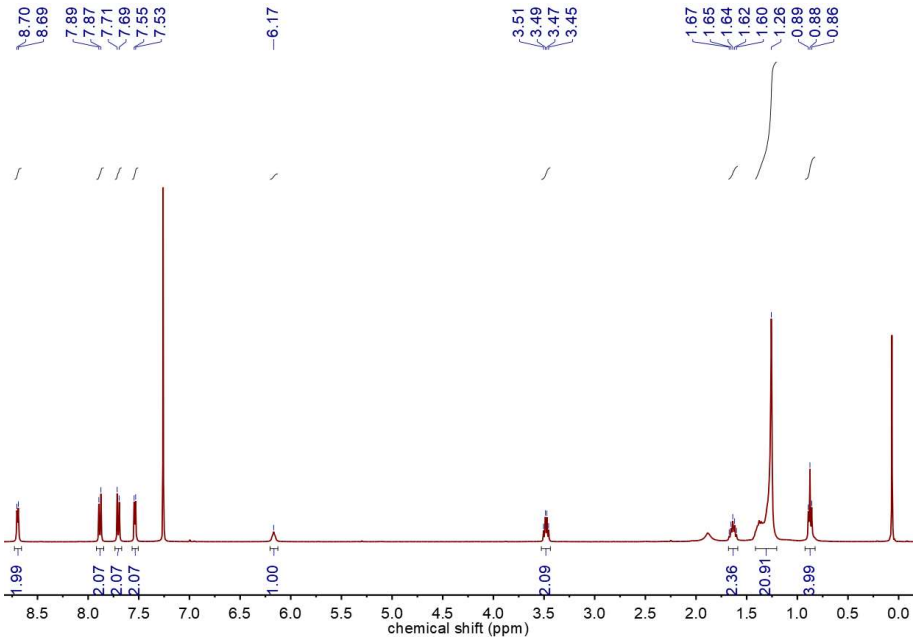

Figure S12. ^{1}H NMR spectrum (400 MHz, $CDCl_3$, 298 K, 2 mM) of the monomer **N12**.

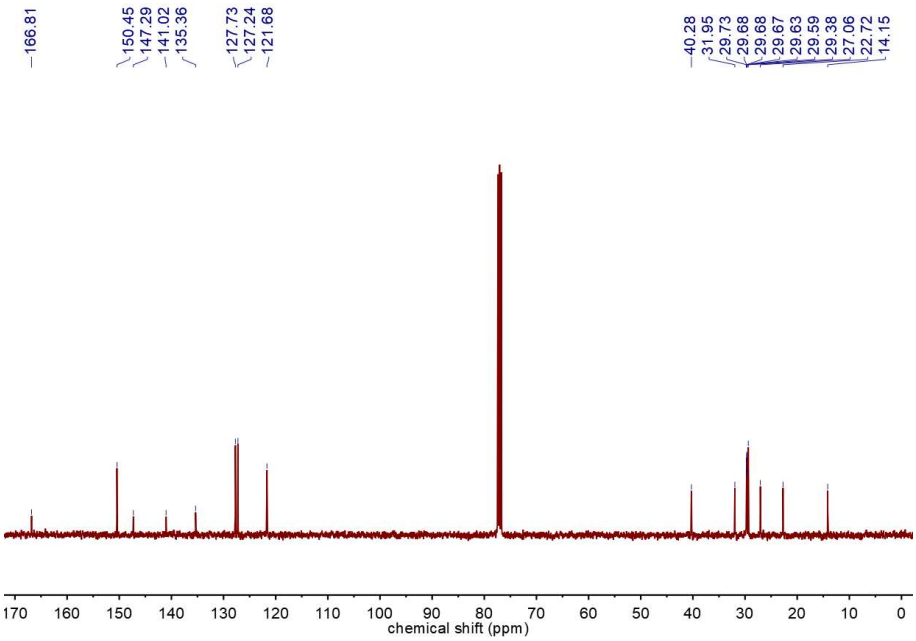

Figure S13. ^{13}C NMR spectrum (101 MHz, $CDCl_3$, 298 K, 15 mM) of the monomer $\mathbf{N_{12}}$.

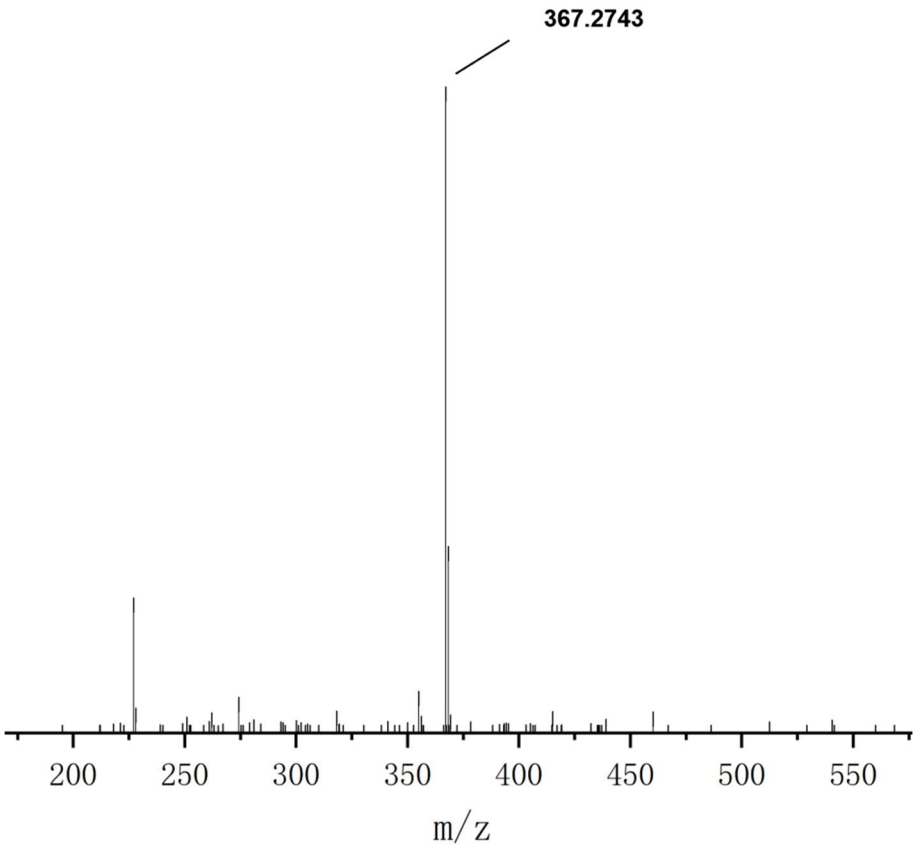

Figure S14. ESI-MS spectrum of the monomer $\mathbf{N_{12}}$.

3. Lewis pairs of the model compounds ***B₁-N₁₁*** *and* ***B₁-N₁₂***

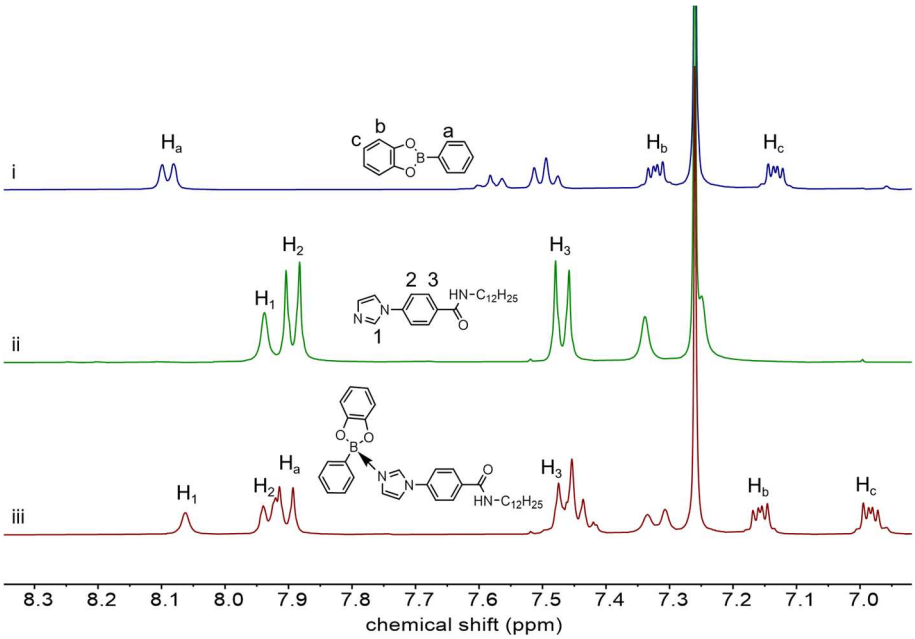

Figure S15. ^{1}H NMR spectra (400 MHz, $CDCl_3$, 298 K, 2 mM) of (i) **B₁**, (ii) **N₁₁** and (iii) the complexation of **B₁-N₁₁**.

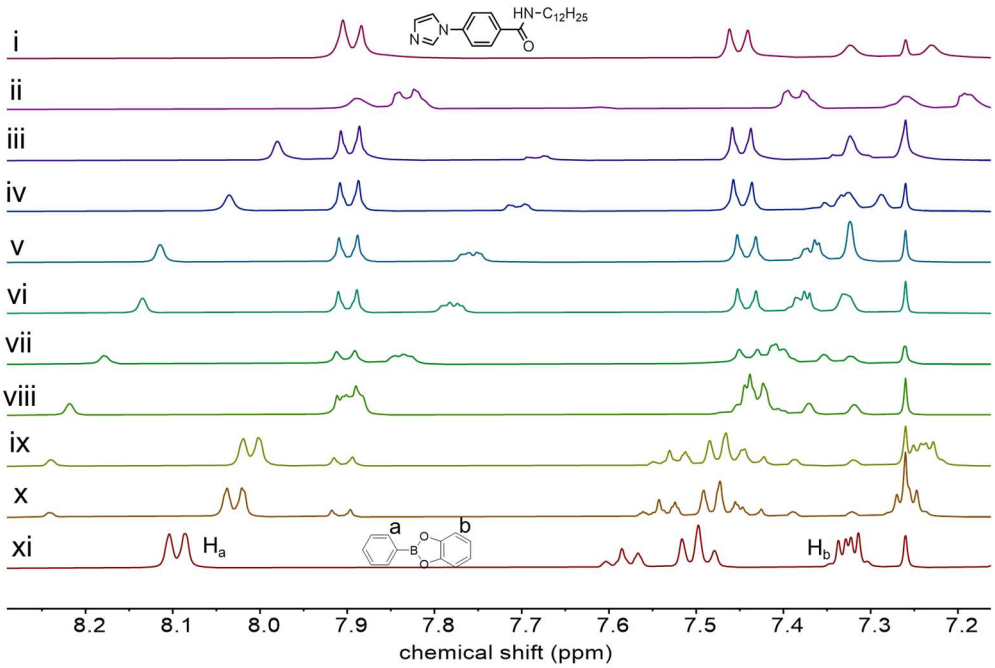

Figure S16. ^{1}H NMR spectra (400 MHz, $CDCl_3$, 298 K) of the Job's plot of **B₁-N₁₁** formed by the complexation of **B₁** and **N₁₁**. The total concentration of **B₁** and **N₁₁** is fixed: [**B₁**] + [**N₁₁**] = 10 mM. (i) [**N₁₁**] = 10 mM, (ii–x) [**N₁₁**]:[**B₁**] = 9:1, 8:2, 7:3, 6:4, 5:5, 4:6, 3:7, 2:8, 1:9, (xi) [**B₁**] = 10 mM.

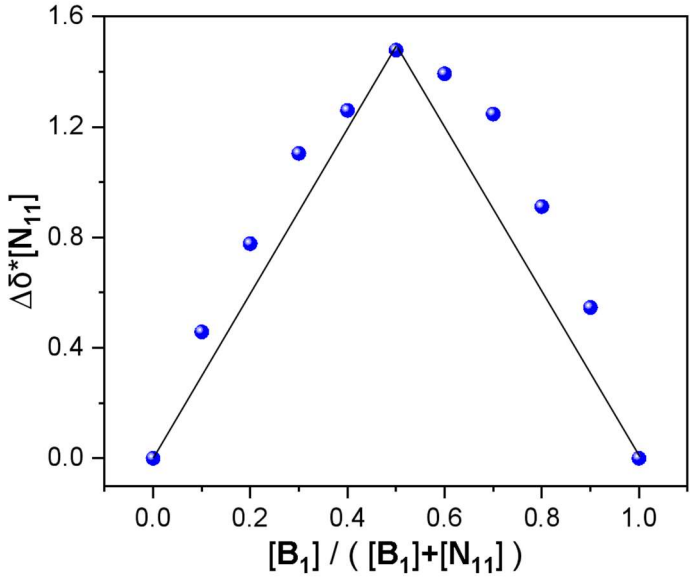

Figure S17. Job's plot obtained by plotting the chemical shift change of the $\mathbf{B_1}$'s proton H_a in ^{1}H NMR spectra by varying the ratio of $\mathbf{B_1}$ and $\mathbf{N_{11}}$ against the mole fraction of $\mathbf{B_1}$. The total concentration is fixed: [$\mathbf{B_1}$] + [$\mathbf{N_{11}}$] = 10 mM.

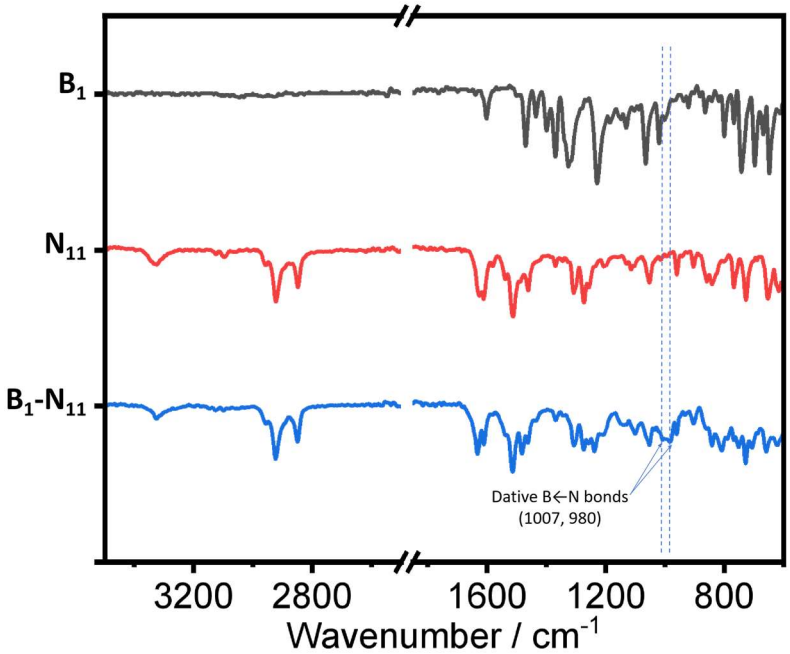

Figure S18. Infrared spectra of $\mathbf{B_1}$, $\mathbf{N_{11}}$ and $\mathbf{B_1}$-$\mathbf{N_{11}}$. The wavenumbers at 1007 cm^{-1} and 980 cm^{-1} corresponds to the characteristic absorption peak of the dative B←N bonds.

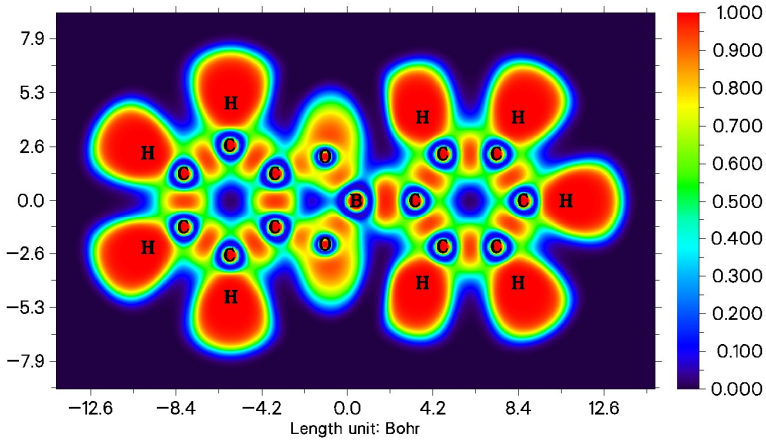

Figure S19. Color-filled maps of ELF of $\mathbf{B_1}$.

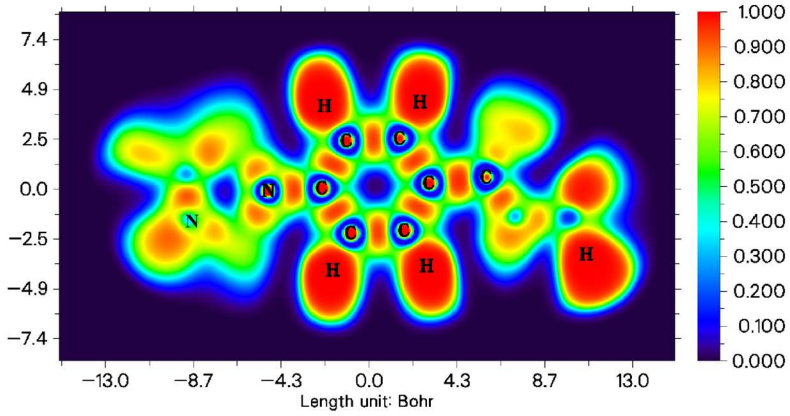

Figure S20. Color-filled maps of ELF of $\mathbf{N_{11}}$.

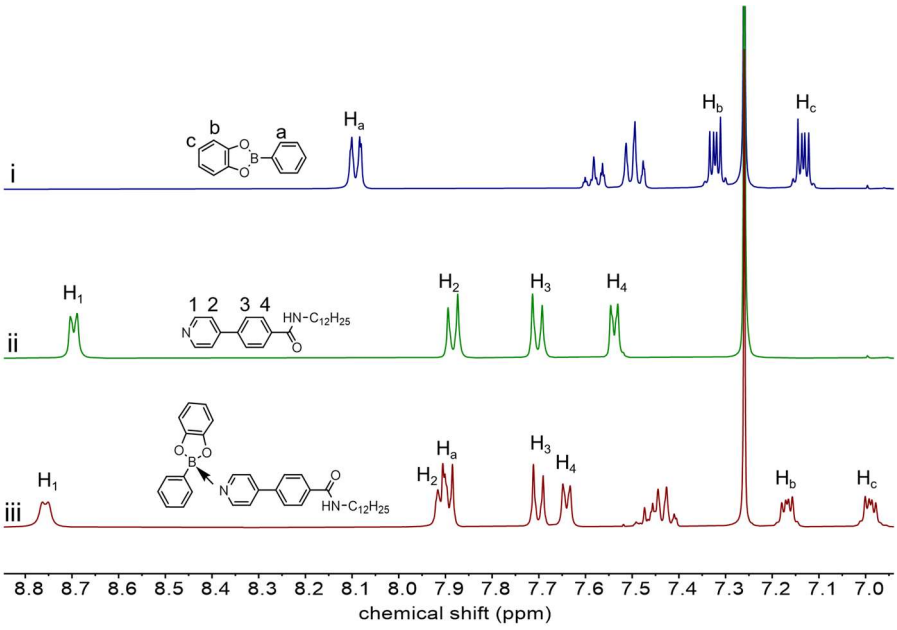

Figure S21. ^{1}H NMR spectra (400 MHz, $CDCl_3$, 298 K, 2 mM) of (i) $\mathbf{B_1}$, (ii) $\mathbf{N_{12}}$ and (iii) the complexation of $\mathbf{B_1}$-$\mathbf{N_{12}}$.

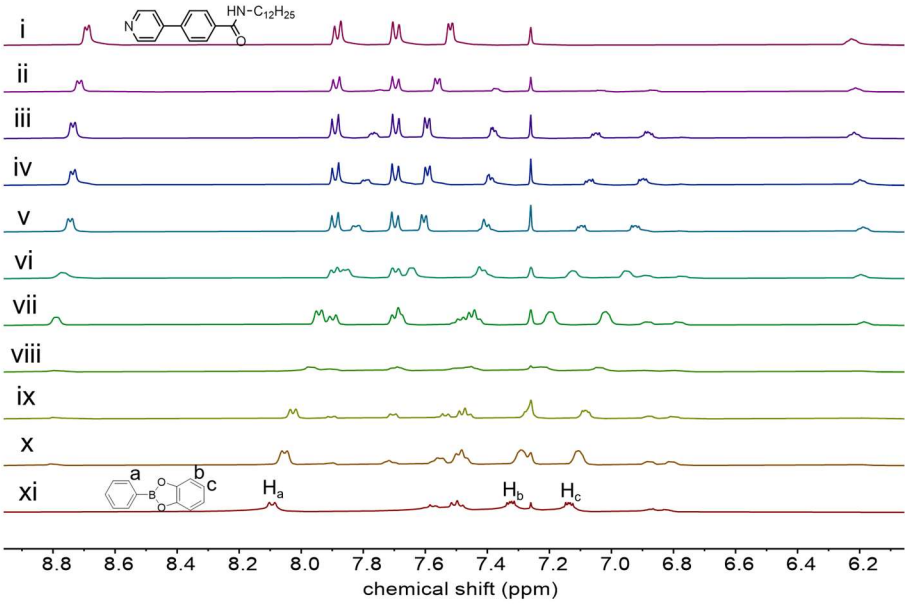

Figure S22. ^{1}H NMR spectra (400 MHz, $CDCl_3$, 298 K) of the Job's plot of **B₁-N₁₂** formed by the complexation of **B₁** and **N₁₂**. The total concentration of **B₁** and **N₁₂** is fixed: [**B₁**] + [**N₁₂**] = 10 mM. (i) [**N₁₂**] = 10 mM, (ii–x) [**N₁₂**]:[**B₁**] = 9:1, 8:2, 7:3, 6:4, 5:5, 4:6, 3:7, 2:8, 1:9, (xi) [**B₁**] = 10 mM.

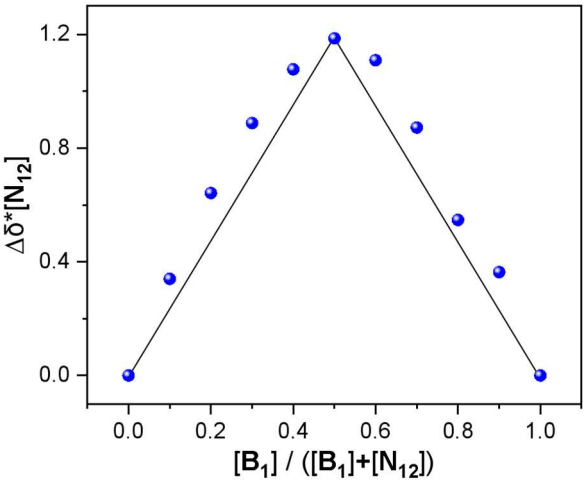

Figure S23. Job's plot obtained by plotting the chemical shift change of **B₁**'s proton H_c in ^{1}H NMR spectra by varying the ratio of **B₁** and **N₁₂** against the mole fraction of **B₁**. The total concentration is fixed: [**B₁**] + [**N₁₂**] = 10 mM.

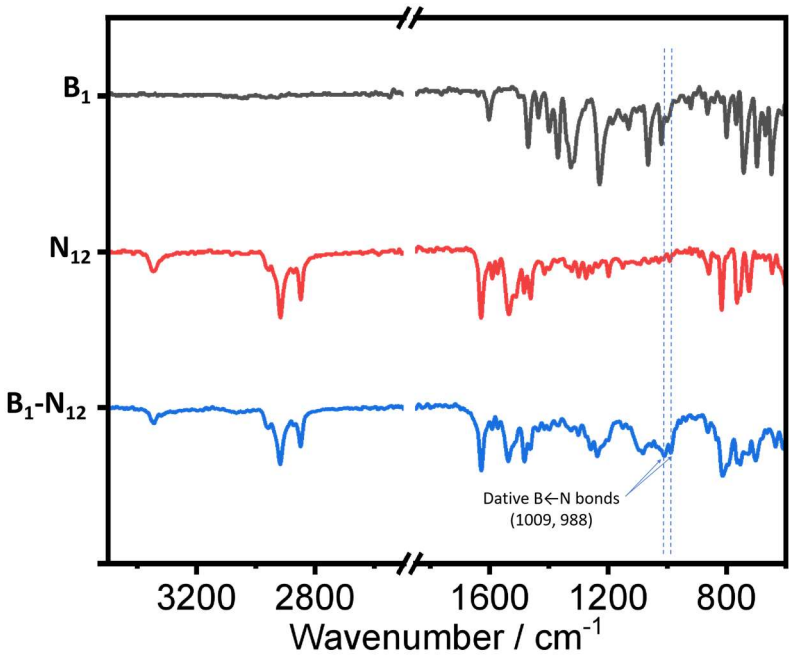

Figure S24. Infrared spectra of **B₁**, **N₁₂** and **B₁-N₁₂**. The wavenumbers at 1009 cm^{-1} and 988 cm^{-1} corresponds to the characteristic absorption peak of the dative B←N bonds.

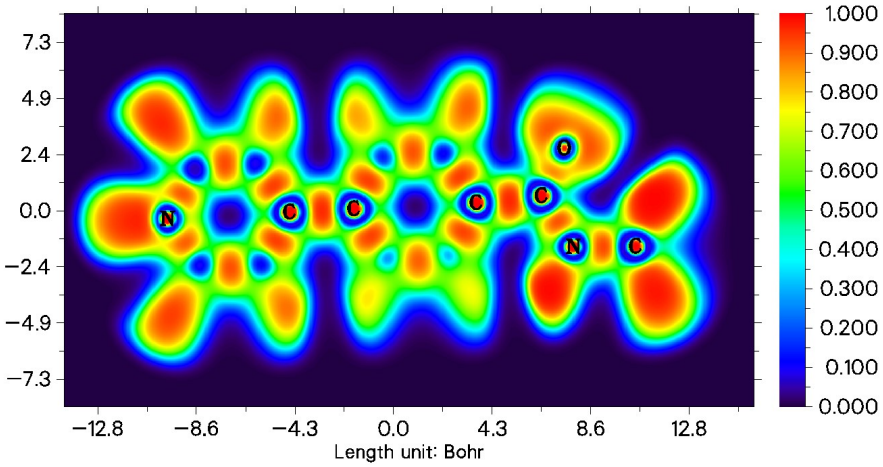

Figure S25. Color-filled maps of ELF of **N₁₂**.

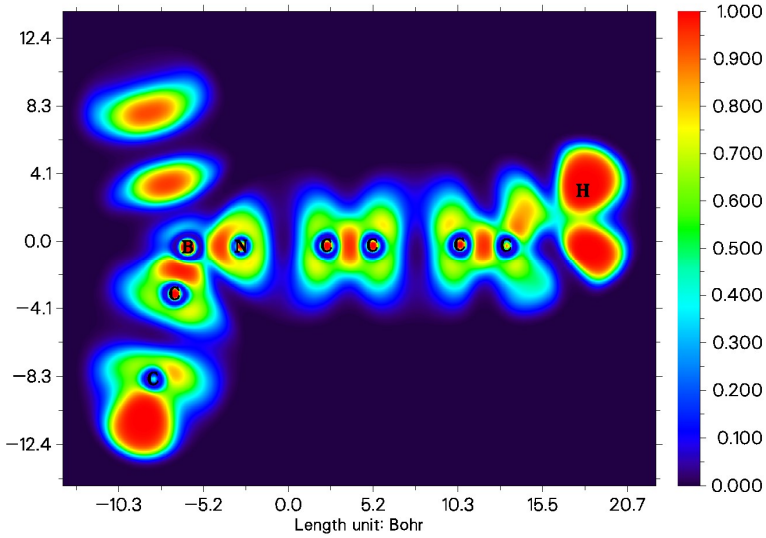

Figure S26. Color-filled maps of ELF of $\mathbf{B_1}$-$\mathbf{N_{12}}$. There is a large ELF value between the B and N atoms, which means that a new chemical bond has been formed between the B and N atoms and that the bond energy of this new chemical bond is large.

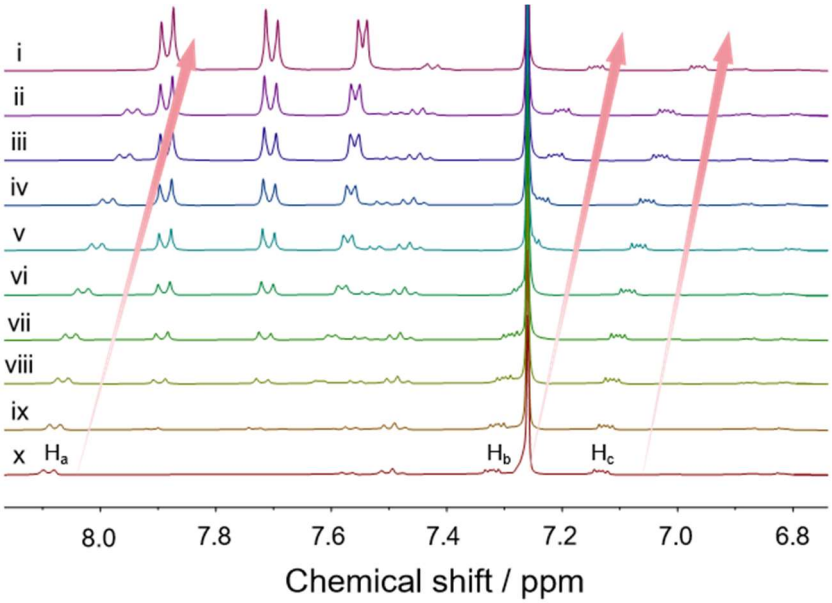

Figure S27. ^{1}H NMR titration (400 MHz, $CDCl_3$, 298 K) of complex $\mathbf{B_1}$-$\mathbf{N_{12}}$ in $CDCl_3$. The concentration of $\mathbf{N_{12}}$ gradually increased: (x) 0, (ix) 0.4, (viii) 1.0, (vii) 1.4, (vi) 2.0, (v) 2.8, (iv) 3.4, (iii) 4.2, (ii) 5.6, (i) 10 mM. The concentration of $\mathbf{B_1}$ was constant to 2.0 mM. The arrows showed the chemical shifts of aromatic region in $\mathbf{B_1}$.

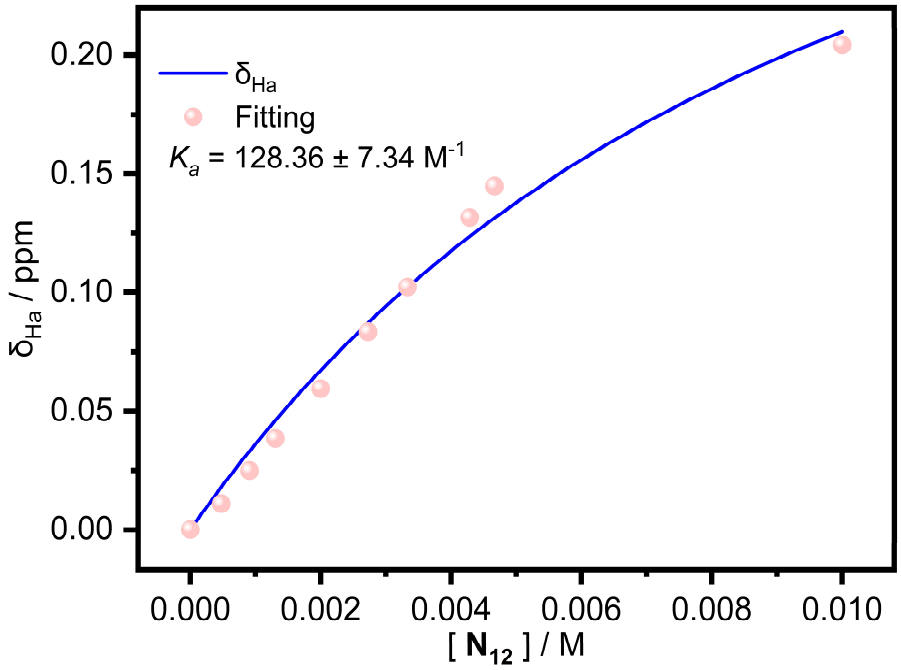

Figure S28. Binding isotherm of the **B₁-N₁₂**. Borate aromatic signals were monitored and fitted using a 1:1 binding equilibrium equation.

*4. Formation of the **MCSP₁** and **MCSP₂***

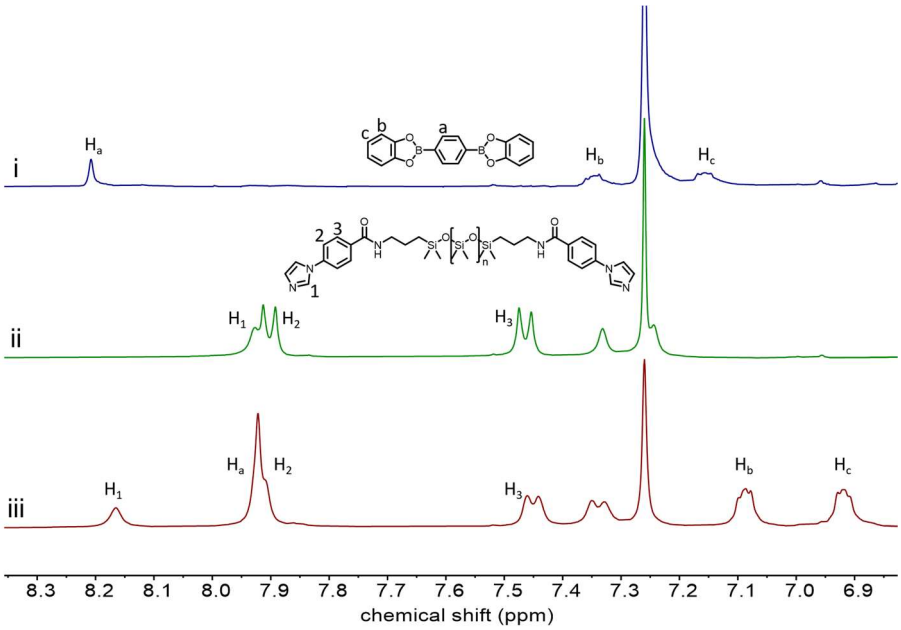

Figure S29. ^{1}H NMR spectra (400 MHz, $CDCl_3$, 298 K, 2 mM) of (i) **B₂**, (ii) **N₂₁** and (iii) **MCSP₁**.

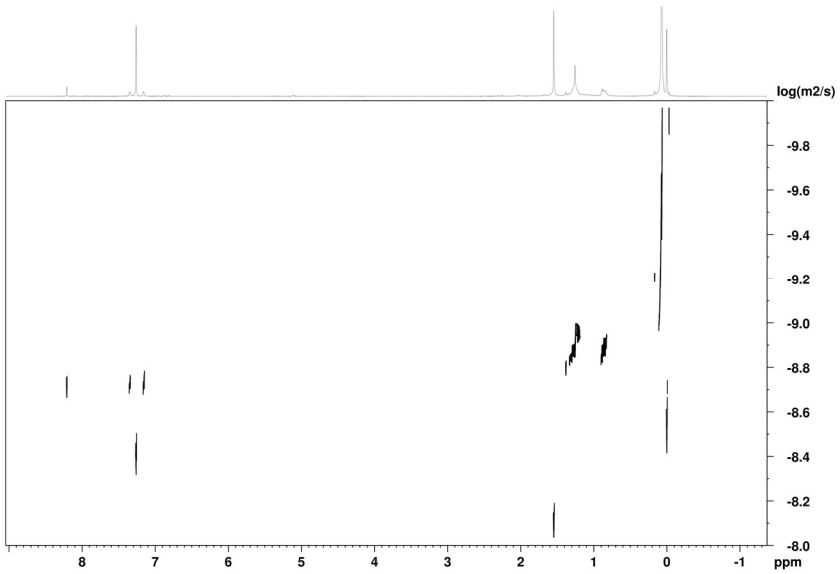

Figure S30. DOSY spectrum (600 MHz, $CDCl_3$, 298 K, 2 mM) of **B₂**. Diffusion coefficient of **B₂** is 1.83×10^{-9} m^2/s.

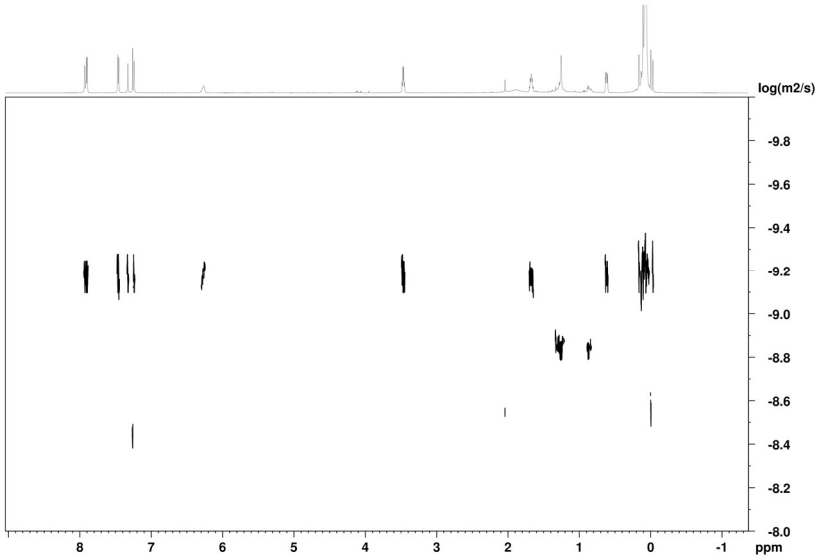

Figure S31. DOSY spectrum (600 MHz, $CDCl_3$, 298 K, 2 mM) of $\mathbf{N_{21}}$. Diffusion coefficient of $\mathbf{N_{21}}$ is 6.89×10^{-10} m^2/s.

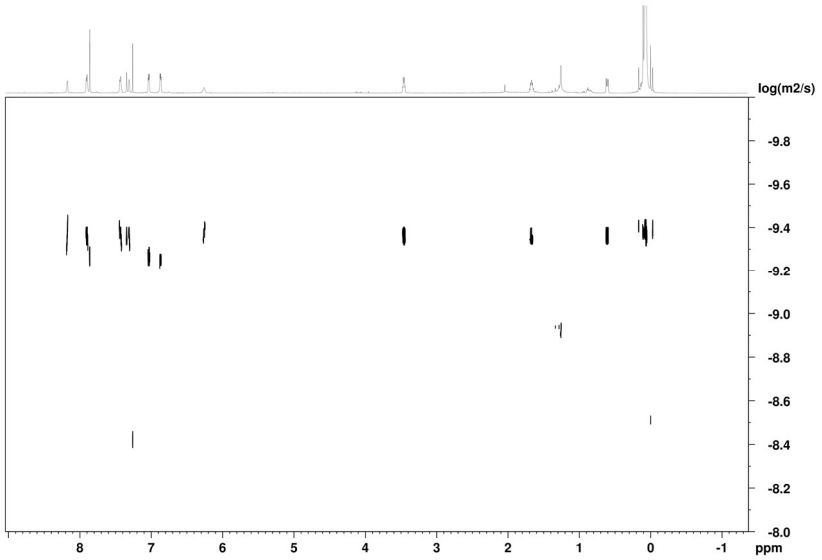

Figure S32. DOSY spectrum (600 MHz, $CDCl_3$, 298 K, 2 mM) of $\mathbf{MCSP_1}$. Diffusion coefficient of $\mathbf{MCSP_1}$ is 3.88×10^{-10} m^2/s.

Table S1. GPC data of $\mathbf{N_{21}}$, $\mathbf{N_{22}}$, $\mathbf{MCSP_1}$, $\mathbf{MCSP_2}$, $\mathbf{MCSP_1}^a$ and $\mathbf{MCSP_1}^b$.

	M_n	M_w	M_z	PDI
$\mathbf{N_{21}}$	2457	2551	2674	1.04
$\mathbf{N_{22}}$	2469	2543	2648	1.03
$\mathbf{MCSP_1}$	10325	12089	14377	1.17
$\mathbf{MCSP_2}$	3048	3372	3850	1.11
$\mathbf{MCSP_1}^a$	10250	12020	14280	1.17
$\mathbf{MCSP_1}^b$	9180	10950	12190	1.18

[a] **MCSP$_1$** after two TFA/TEA cycles. [b] **MCSP$_1$** after two TBAF/BTE cycles.

The results revealed that **MCSP$_1$** exhibited a significantly higher molecular weight (M_z = 14377) and polydispersity index (PDI = 1.17) compared to its counterpart compound **N$_{21}$** (M_z = 2674, PDI = 1.04), indicating the successful formation of extended polymer chains. In contrast, **MCSP$_2$** displayed a relatively low molecular weight (M_z = 3850) and PDI (1.11) compared to **MCSP$_1$**. These observations suggest that the dative B←N bonds between **N$_{22}$** and **B$_2$** may lack the strength required to maintain the long polymer chains under GPC conditions. Notably, this outcome aligns with the designed modulation of coordination strength through the tuning of Lewis acidity and basicity, providing valuable insights into the relationship between molecular design and polymerization behaviors. This phenomenon reflects that the enhanced binding affinity of noncovalent repeat units is essential for the formation of large-sized supramolecular polymers.

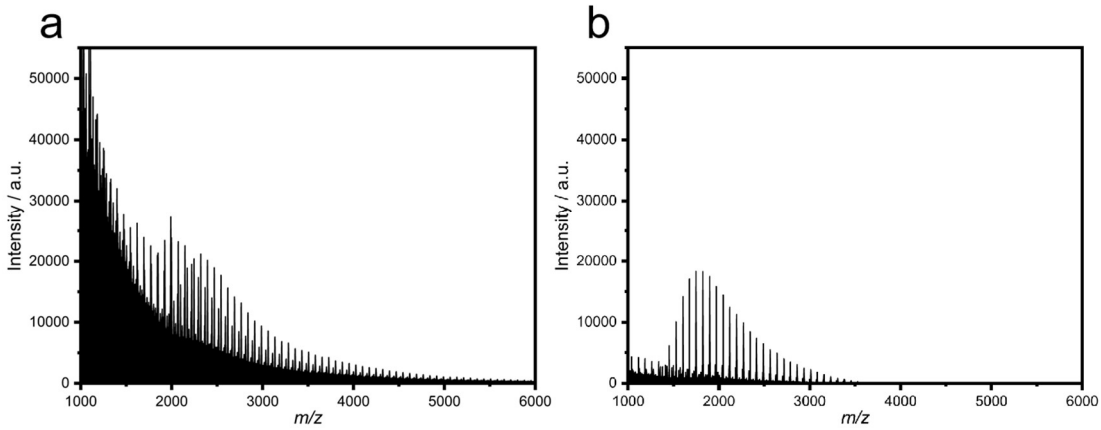

Figure S33. MALDI-TOF-MS spectra of (a) **MCSP$_1$** and (b) **MCSP$_2$**. As evidenced by the MALDI-TOF-MS analyses of **MCSP$_1$** and **MCSP$_2$**, dative B←N bonds under high-energy ionization conditions imposes significant constraints on stabilizing extended supramolecular polymer chains. Fragmentation patterns in the spectra indicate partial scission of PDMS backbones, suggesting susceptibility of siloxane linkages to collisional activation. Unfortunately, the absence of characteristic isotopic distributions or mass intervals corresponding to cyclic topologies precludes definitive identification of macrocyclic architectures in these assemblies. Even so, we speculated that cyclic species are hard to exist in this supramolecular polymerization system. Firstly, one of the components of the obtained **MCSP$_1$** or **MCSP$_2$** is PDMS. The unfolded long chains of PDMS in the good solvent of $CHCl_3$ prevent the formation of cyclic species in the supramolecular polymerization process. Secondly, the concentration of the supramolecular polymerization is set relatively high in this work, which could also restrain cyclization according to the ring-chain transition mechanism.[5,6]

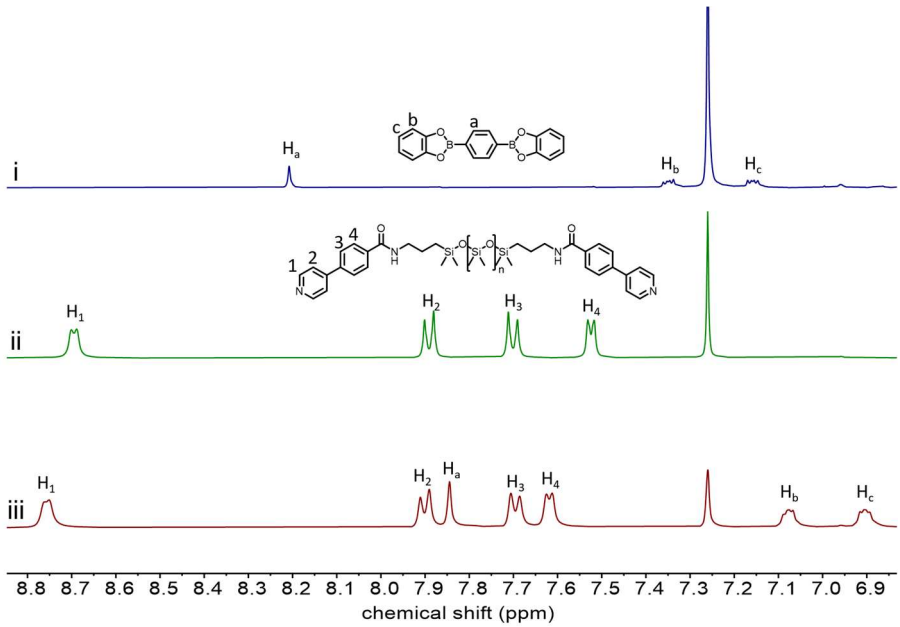

Figure S34. ^{1}H NMR spectra (400 MHz, $CDCl_3$, 298 K, 2 mM) of (i) **B$_2$**, (ii) **N$_{22}$** and (iii) **MCSP$_2$**.

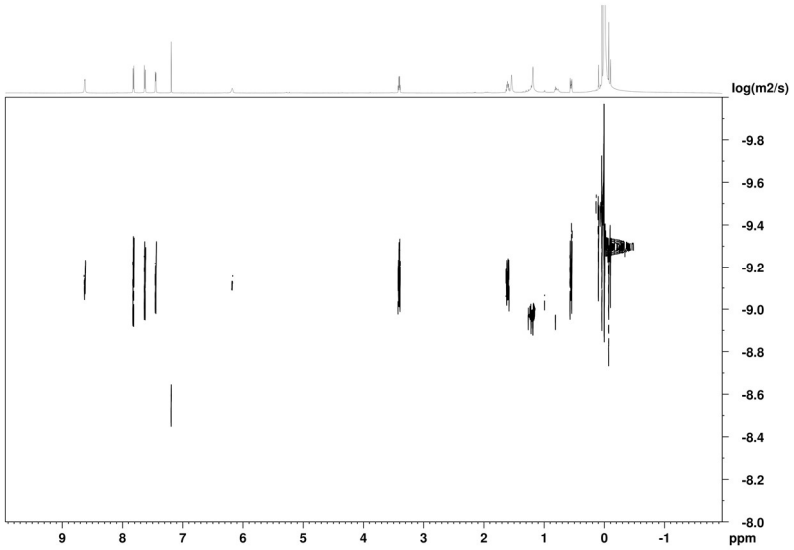

Figure S35. DOSY spectrum (600 MHz, $CDCl_3$, 298 K, 2 mM) of $\mathbf{N_{22}}$. Diffusion coefficient of $\mathbf{N_{22}}$ is 1.14×10^{-9} m^2/s.

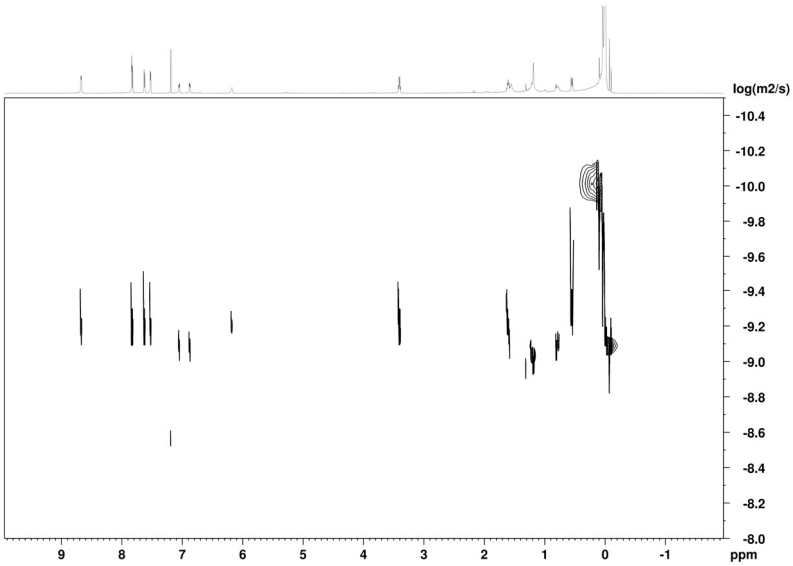

Figure S36. DOSY spectrum (600 MHz, $CDCl_3$, 298 K, 2 mM) of $\mathbf{MCSP_2}$. Diffusion coefficient of $\mathbf{MCSP_2}$ is 6.04×10^{-10} m^2/s.

*5. Intrinsic stimuli-responsiveness of the **MCSP$_1$** and **MCSP$_2$***

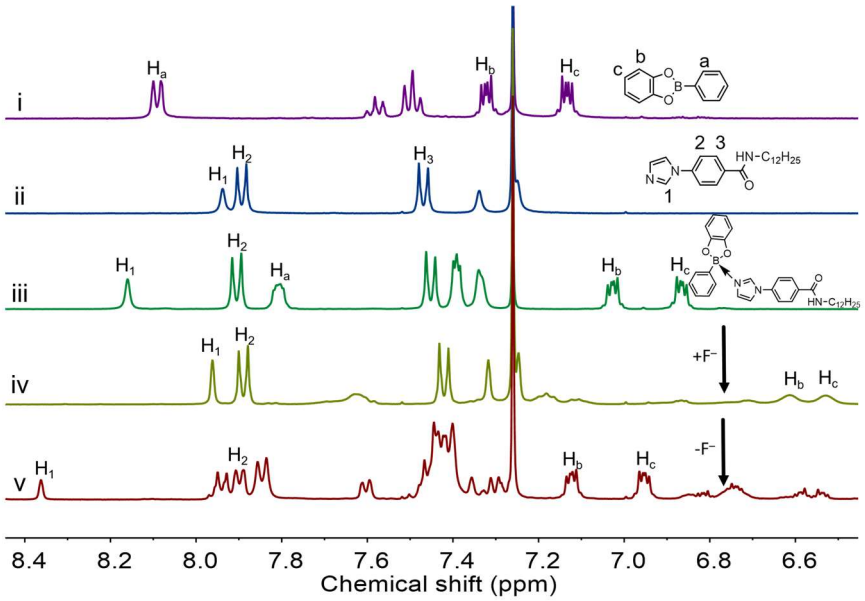

Figure S37. ^{1}H NMR spectra (400 MHz, $CDCl_3$, 298 K, 2 mM) of TBAF/BTE induced fluoridating/defluoridating **B$_1$** in **B$_1$-N$_{11}$**: (i) **B$_1$**, (ii) **N$_{11}$**, (iii) **B$_1$-N$_{11}$**, (iv) **B$_1$-N$_{11}$** after the addition of TBAF and then (v) **B$_1$-N$_{11}$** after the addition of equal amounts of BTE.

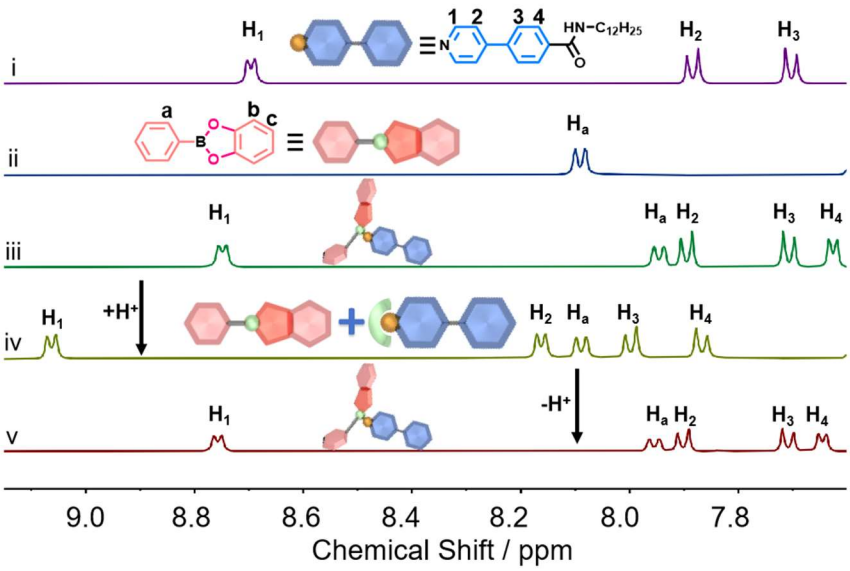

Figure S38. ^{1}H NMR spectra (400 MHz, $CDCl_3$, 298 K, 2 mM) of TFA/TEA induced protonating/deprotonating **N$_{12}$** in **B$_1$-N$_{12}$**: (i) **N$_{12}$**, (ii) **B$_1$**, (iii) **B$_1$-N$_{12}$**, (iv) **B$_1$-N$_{12}$** after the addition of TFA and then (v) after the addition of equal amounts of TEA.

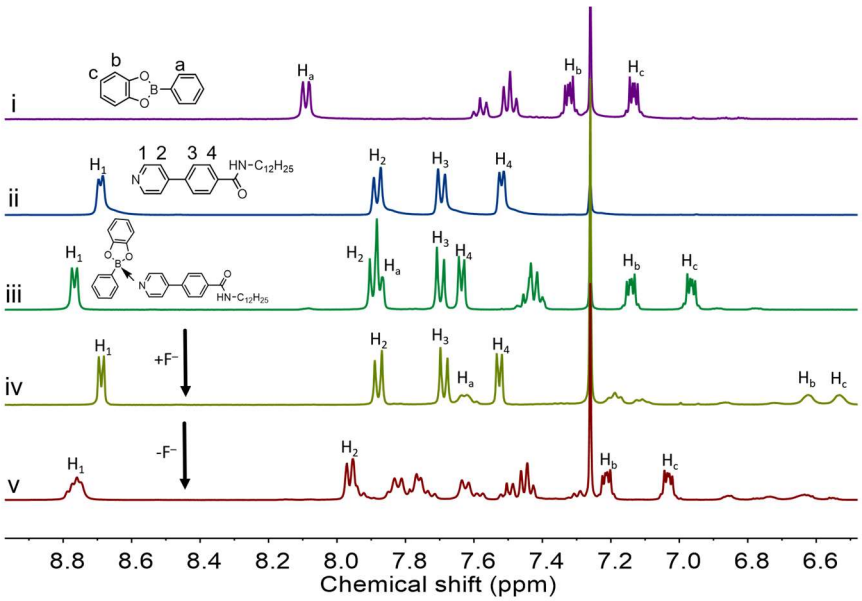

Figure S39. ^{1}H NMR spectra (400 MHz, $CDCl_3$, 298 K, 2 mM) of TBAF/BTE induced fluoridating/defluoridating **B₁** in **B₁-N₁₂**: (i) **B₁**, (ii) **N₁₂**, (iii) **B₁-N₁₂**, (iv) **B₁-N₁₂** after the addition of TBAF and then (v) **B₁-N₁₂** after the addition of equal amounts of BTE.

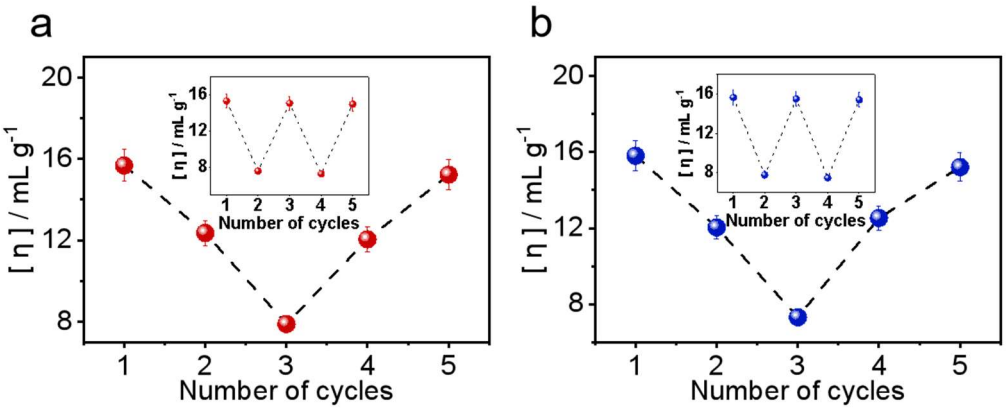

Figure S40. (a) Changes in [η] of **MCSP₂** with the addition of TFA/TEA (1–3, the addition of TFA; 3–5, the addition of TEA). Inset shows the cycle plots of protonating/deprotonating **N₂₂** in **MCSP₂** (50 mg/mL, $CHCl_3$, 298 K). (b) Changes in [η] of **MCSP₂** with the addition of TBAF/BTE (1–3, the addition of TBAF; 3–5, the addition of BTE). Inset shows the cycle plots of the fluoridating/defluoridating **B₂** in **MCSP₂** (50 mg/mL, $CHCl_3$, 298 K).

References

[1] Gaussian 09, Revision A.02, M. J. Frisch, G. W. Trucks, H. B. Schlegel, G. E. Scuseria, M. A. Robb, J. R. Cheeseman, G. Scalmani, V. Barone, B. Mennucci, G. A. Petersson, H. Nakatsuji, M. Caricato, X. Li, H. P. Hratchian, A. F. Izmaylov, J. Bloino, G. Zheng, J. L. Sonnenberg, M. Hada, M. Ehara, K. Toyota, R. Fukuda, J. Hasegawa, M. Ishida, T. Nakajima, Y. Honda, O. Kitao, H. Nakai, T. Vreven, J. A. Montgomery, Jr., J. E. Peralta, F. Ogliaro, M. Bearpark, J. J. Heyd, E. Brothers, K. N. Kudin, V. N. Staroverov, R. Kobayashi, J. Normand, K. Raghavachari, A. Rendell, J. C. Burant, S. S. Iyengar, J. Tomasi, M. Cossi, N. Rega, J. M. Millam, M. Klene, J. E. Knox, J. B. Cross, V. Bakken, C. Adamo, J. Jaramillo, R. Gomperts, R. E. Stratmann, O. Yazyev, A. J. Austin, R. Cammi, C. Pomelli, J. W. Ochterski, R. L. Martin, K. Morokuma, V. G. Zakrzewski, G. A. Voth, P. Salvador, J. J. Dannenberg, S. Dapprich, A. D. Daniels,O. Farkas, J. B. Foresman, J. V. Ortiz, J. Cioslowski, and D. J. Fox, *Gaussian, Inc.,* 2009, *Wallingford CT*.

[2] Y. Zhao and D. G. Truhlar, *Theor. Chem. Acc.,* 2008, **120**, 215–241.

[3] S. Grimme, S. Ehrlich and L. Goerigk, *J. Comput. Chem.,* 2011, **32**, 1456–1465.

[4] G. Y. Lee, E. Hu, A. L. Rheingold, K. N. Houk and E. M. Sletten, *J. Org. Chem.,* 2021, **86**, 8425–8436.

[5] Y.-K. Tian, Y.-G. Shi, Z.-S. Yang and F. Wang, *Angew. Chem. Int. Ed.,* 2014, **53**, 6090–6094.

[6] T. F. A. De Greef, M. M. J. Smulders, M. Wolffs, A. P. H. J. Schenning, R. P. Sijbesma and E. W. Meijer, *Chem. Rev.,* 2009, **109**, 5687–5754.